nature communications

Article

https://doi.org/10.1038/s41467-024-55715-8

Earthworm inspired lubricant self-pumping hydrogel with sustained lubricity at high loading

Received: 7 June 2024

Accepted: 23 December 2024

Published online: 04 January 2025

Check for updates

Shuanhong Ma[1,2,4], Lunkun Liu[1,3,4], Weiyi Zhao[1], Renjie Li[1], Xiaoduo Zhao[1,2], Yunlei Zhang[1], Bo Yu[1], Ying Liu[3] ✉ & Feng Zhou[1] ✉

The development of mechanically robust super-lubrication hydrogel materials with sustained lubricity at high contact pressures is challenging. In this work, inspired by the durable lubricity feature of the earthworm epidermis, a multilevel structural super-lubrication hydrogel (MS-SLH) system, the so-called lubricant self-pumping hydrogel, is developed. The MS-SLH system is manufactured by chemically dissociating a double network hydrogel to generate robust and wrinkled lubrication layer, and then laser etching was used to generate cylindrical texture pores as gland-like pockets for storing lubricants. The surface of MS-SLH system shows ultrafast hydration characteristics and reversible pore-closing and pore-opening behavior. The current MS-SLH system shows excellent SL features, as follows: a very low COF (~0.0079) at high contact pressure condition (*P:* 11.32 MPa); a stable and robust SL lifespan (COF: ~0.0028, *P*: 8.48 MPa, 100k cylces) without surface wear; and a sustained lubricity period (3700 cycles) with limited lubricant volume (5 µL) in air. The robust and sustained lubricity of the MS-SLH system is likely attributed to the synergy from the strong electrostatic repulsion effect at the sliding interface, the robust but compliant modulus of the dissociation lubrication layer, and the self-pumping lubricant release from the gland-like pocket of the texture pores during the dynamic shearing process. The demonstration experiments based on self-built equipments intuitively exhibit durable SL behavior of MS-SLH system. This work provides an easy strategy for the large-scale manufacture of high-performance water-lubrication coatings suitable for high-end medical devices or moving parts.

Wet, soft, and slippery features are typical characteristics of biological tissues and organs and involve relative motion. Meanwhile, hydration lubrication is a necessary performance at sliding tissues and organs interfaces.[1,2] For example, a healthy natural cartilage exhibits very low coefficient of friction (COF, ~0.001 to ~0.03) for long service lifetimes (decades) under high contact stress condition (1~20 MPa).[3–5] Hydrogel material systems are potential candidates for simulating those natural tissues and organs to reproduce their lubrication functionality.[6–10] In the past 30 years, scientists have developed numerous methods to construct robust lubricious hydrogel materials as artificial

[1]State Key Laboratory of Solid Lubrication, Lanzhou Institute of Chemical Physics, Chinese Academy of Sciences, Lanzhou, China. [2]Shandong Laboratory of Advanced Materials and Green Manufacture at Yantai, Yantai Zhongke Research Institute of Advanced Materials and Green Chemical Engineering, Yantai, China. [3]School of Advanced Manufacturing, Nanchang University, Nanchang, China. [4]These authors contributed equally: Shuanhong Ma, Lunkun Liu. ✉e-mail: lying@ncu.edu.cn; zhouf@licp.cas.cn

replacement for damaged tissue or organs.[11–16] In addition, the lubrication and load-bearing mechanisms of synthetic hydrogel materials have been systematically studied in order to obtain more realistic biodesign principles.[17–27] According to the classic definition, when the surface COF of synthetic hydrogels is less than 0.01, they are often so-called super-lubrication hydrogels, with the expectation of achieving ultralow wear.

In recent decades, great progress has been made in the preparation of robust super-lubrication hydrogels,[28–35] as well as friction-responsive hydrogel materials.[36–39] Especially, the application exploration of super-lubrication hydrogels coating in the field of medical devices has received unprecedented attention.[40–49] According to the application scenarios of medical devices, the stress tolerance conditions of super lubricating hydrogel coatings are usually different. Currently, the application of super-lubrication hydrogels coating is focused mostly on medical models, catheters and guide wires, and the contact stress is usually very low (below 0.1 MPa). However, for high-end instruments such as artificial joints, the development of matching hydrogel super-lubrication coating is challenging but urgent research topic since the interface contact stress can reach as high as ~10 MPa. Even though tough hydrogels or lubricants-integrated hydrogel systems have been developed, the load-bearing capacity of the current supper-lubrication hydrogel systems for maintaining stable lubricity is still less than 3 MPa, and the lubricity lifespan has not yet exceeded 100,000 cycles. Moreover, due to the inherent dehydration characteristics of hydrogel materials, attaining super-lubrication behavior usually depends on the lubricant bath, while concerns on the lubricity sustainability for a limited number of lubricants in quasi-wet environments have not yet been addressed. Therefore, considering their real application potential as artificial joint coatings, the most urgent challenge of super-lubrication hydrogel systems is to simultaneously achieve ultralow friction, ultrahigh load-bearing and ultralong lifespans with limited lubricant amounts.

In this work, inspired by the durable lubricity feature of earthworm epidermis, a multilevel structural super-lubrication hydrogel (MS-SLH) system, the so-called lubricant self-pumping hydrogel, is developed. The core concept of this system is to create a partially-closed gland-like lubricant pocket to simulate the continuous lubricant migration behavior of epidermis skins and the cartilage layer to achieve dynamic lubricity maintenance. This system successfully realizes robust super-lubrication behavior under high contact pressure conditions (>11 MPa), ultra-long SL lifespans (100,000 cycles), and sustained lubricity in a quasi-wet environment assisted by a trace amount of lubricant (5 μL). This is an excellent SL system, and it provides a key strategy for the large-scale manufacture of high-performance water-lubrication coatings suitable for high-end medical devices and moving parts.

Results

Design concept and preparation of MS-SLH

In nature, earthworms are able to move freely within soil under a squeezing and shearing environment based on the super-slippery epidermis feature, which is closely related to their wrinkled surface microstructures (annuli/microripples) and the continuously secreted aqueous-viscous lubricant from the glands to the epidermis (Fig. 1a), enabling the formation of a typical self-lubrication interface.[50–54] More importantly, this super-slippery feature has considerable robustness and long durability. Inspired by this, a mechanically robust MS-SLH system is manufactured. The specific preparation process of MS-SLH is shown in Fig. 1b. Typically, the double network hydrogel of poly(-acrylamide-acrylic acid)/Fe^{3+} (P(AAm-AA)/Fe) with high mechanical modulus is firstly prepared as mechanically robust matrix (Supplementary Fig. 1). Then, poly(acrylic acid) (PAA) as chemical etchant is used for dissociating the tough network to manufacture the surface lubrication phase (i). Along with the formation of soft dissociated lubrication phase, a periodic but non-regular wrinkled morphology is formed on the surface because of the rising stress difference.[55–57] As a result, the layered super-lubrication hydrogel (SLH) has been engineered. Next, the lubrication phase is exposed to air and undergoes local dehydration, and then laser etching across the lubrication phase (h_1) and substrate matrix (h_2) is used to generate cylindrical texture pores. The manufactured sample is immersed into lubricant bath to allow sufficient swelling and hydration of the dissociation layer (iii). During the dynamic swelling process of the surface dissociation phase, the lubricant (water or macromolecules) spontaneously migrates into the gland-like pocket of the texture pores, accompanied by shrinkage and partial closure of the pores. Finally, the earthworm-inspired MS-SLH sample is successfully prepared. As expected, the wrinkled lubrication phase of MS-SLH could generate a strong hydration layer to decrease the local interface friction force, whereas lubricant confined within the pores maintains the lubricity lifespan of the system under the dynamic shearing process. As a concept demonstration, an artificial SLH earthworm with a length of 36 cm is manufactured (Fig. 1c), while the fluorescence imaging clearly reveals the existence of a hydrated dissociation lubrication phase, and the wrinkled pattern is clearly observed. Interestingly, the manufacture of SL wrinkled patterns can be completely controlled by using a designed mask to selectively dissociate the lubrication phase (Fig. 1d). Our current MS-SLH system shows excellent SL features, such as a very low COF (~0.0079) at high contact pressure (P) condition (11.32 MPa), a stable and robust SL lifespan (COF: ~0.0028, P: 8.48 MPa, 100 k cycles) without surface wear, and a sustained lubricity period (3700 cycles) with a limited lubricant (5 μL) in air.

Characterizations of SLH

The generation of a dissociation layer causes the original double-network hydrogel to appear as opaque along with the decrease of transmittance (Fig. 2b), while the symbolic formulas, logos, and landscapes are not clearly observed (Fig. 2a). Compared with the dense network of the original double-network hydrogel (Supplementary Figs. 2–4), the dissociation layer exhibits a typical porous structure (Fig. 2c). The dissociation layer and substrate phase are tightly combined to form a typically layered structure (Fig. 2d), and the SLH sample is successfully obtained. The generation of the dissociation layer is dominated by a weak acid-assisted de-coordination strategy (Supplementary Fig. 5). Specifically, with the erosion of the PAA polymer chains, the strong coordination bonds between the carboxylate ions and iron ions (-COO^-—Fe^{3+}) within the double-network hydrogel are disrupted. At the same time, the dissociated H^+ ions from PAA is likely exchanged with the de-coordinated carboxylate ions (-COO^-) to form carboxylate groups (-COOH). This deduction can be confirmed by observing the enhanced carbon (C) and oxygen (O) elements signals as well as the weakened iron (Fe) element signals via energy-dispersive X-ray spectroscopy (EDS) mapping (Supplementary Figs. 6-7). Due to its porous structure, the SLH sample shows excellent surface hydration capacity and demonstrates good anti-fouling functionality. In typical cases, the as-manufactured artificial SLH earthworms show low adhesion for the dyed vegetable oil (Fig. 2e), whereas the viscous heavy oil adhered onto the surface can be easily washed away by water (Fig. 2f). The strong hydration capacity of SLH can be further confirmed by the dynamic wetting process of the water droplet (Fig. 2g). Compared with control sample, water droplet can fully spread on the surface of the dissociation layer for SLH sample within 30 sec.

Lubrication performance of SLH

The wet morphologies of the periodic wrinkles on the surface of the dissociation layer evolve dynamically with increasing PAA mass concentration and dissociation time (Supplementary Figs. 8, 9). The thickness of the dissociation layer can also be precisely tuned by

https://doi.org/10.1038/s41467-024-55715-8

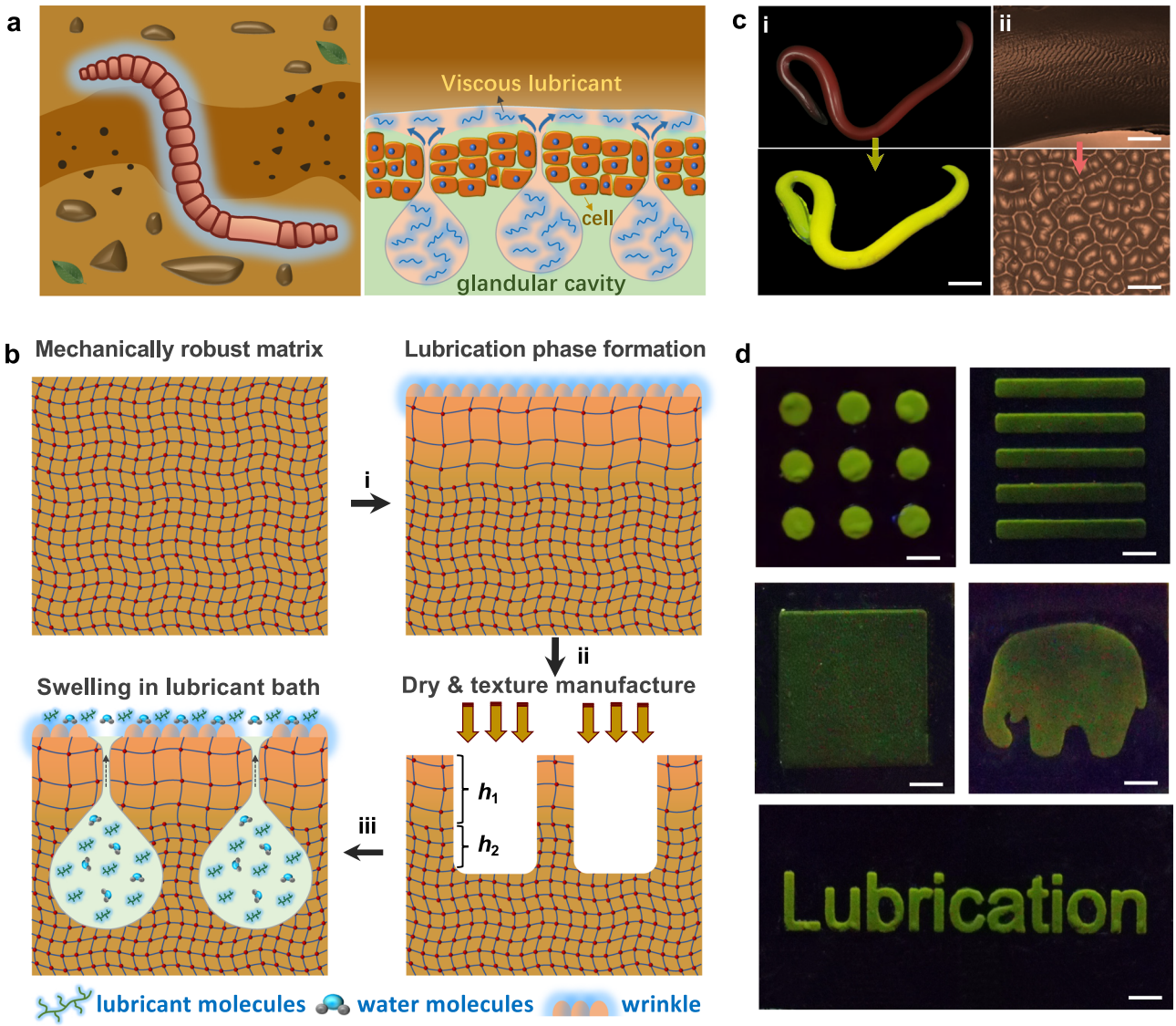

Fig. 1 | Preparation of multilevel structured super-lubrication hydrogel (MS-SLH). a Lubrication secrets of earthworms: the surface is coated with a lubricating layer in the soil (left), which is composed of hydrated viscous protein molecules secreted from cells or glands (right). **b** Manufacturing process of MS-SLH: (i) formation of a wrinkled lubrication phase on the surface of a mechanically robust DN-hydrogel, (ii) partial dehydration and laser-assisted manufacturing of a surface cylindrical texture array ($h = h_1 + h_2$, h_1 represents the etching length of the lubrication phase, h_2 represents the etching length of the robust DN-hydrogel matrix), and (iii) sufficient swelling in the lubricant bath and formation of a gland-like pocket for sealing the amount of lubricant. **c** Manufacturing of artificial MS-SLH earthworms: (i) real photograph (top) and fluorescence image (bottom, scale: 4 cm) of the MS-SLH earthworms and (ii) optical microscope images showing the local (top, scale: 4 mm) and enlarged (bottom, scale: 200 μm) wrinkled micromorphology of the MS-SLH earthworms. **d** Manufacture of the MS-SLH patterns (dot array, strip array, square, elephant symbol, "lubrication" word); the scales for all patterns are the same (4 mm) on the surface of the mechanically robust DN-hydrogel.

controlling the PAA mass concentration and dissociation time (Supplementary Figs. 10, 11). As the dissociation time increased, the thickness of the dissociation layer initially increases and then decreases, and a maximum is reached at 10% PAA concentration (Fig. 3a). Correspondingly, the change of elastic modulus shows an opposite trend to that of the thickness evolution (Fig. 3c). As the dissociation time increases, the thickness and network pore size of the dissociation layer gradually increases (Fig. 3b), whereas the elastic modulus of the dissociation layer gradually decreases (Fig. 3d). Furthermore, the contact angle, water content, surface roughness and single island area from wrinkles of dissociation layer for the SLH samples are measured (Supplementary Figs. 12–21), for which follow the similar evolution trend as that of thickness and elastic modulus. Also, it is found that the dissociation layer exhibits fast hydration process and the entire hydration/dehydration process is completely reversible (Supplementary Fig. 22). These results indicate that dissociation is a dynamic swelling and hydration process of the original double network hydrogel substrate, and a decrease in the mechanical modulus is observed because of the increased network pore sizes (Supplementary Figs. 23, 24). Considering the balance between hydration degree of the

https://doi.org/10.1038/s41467-024-55715-8

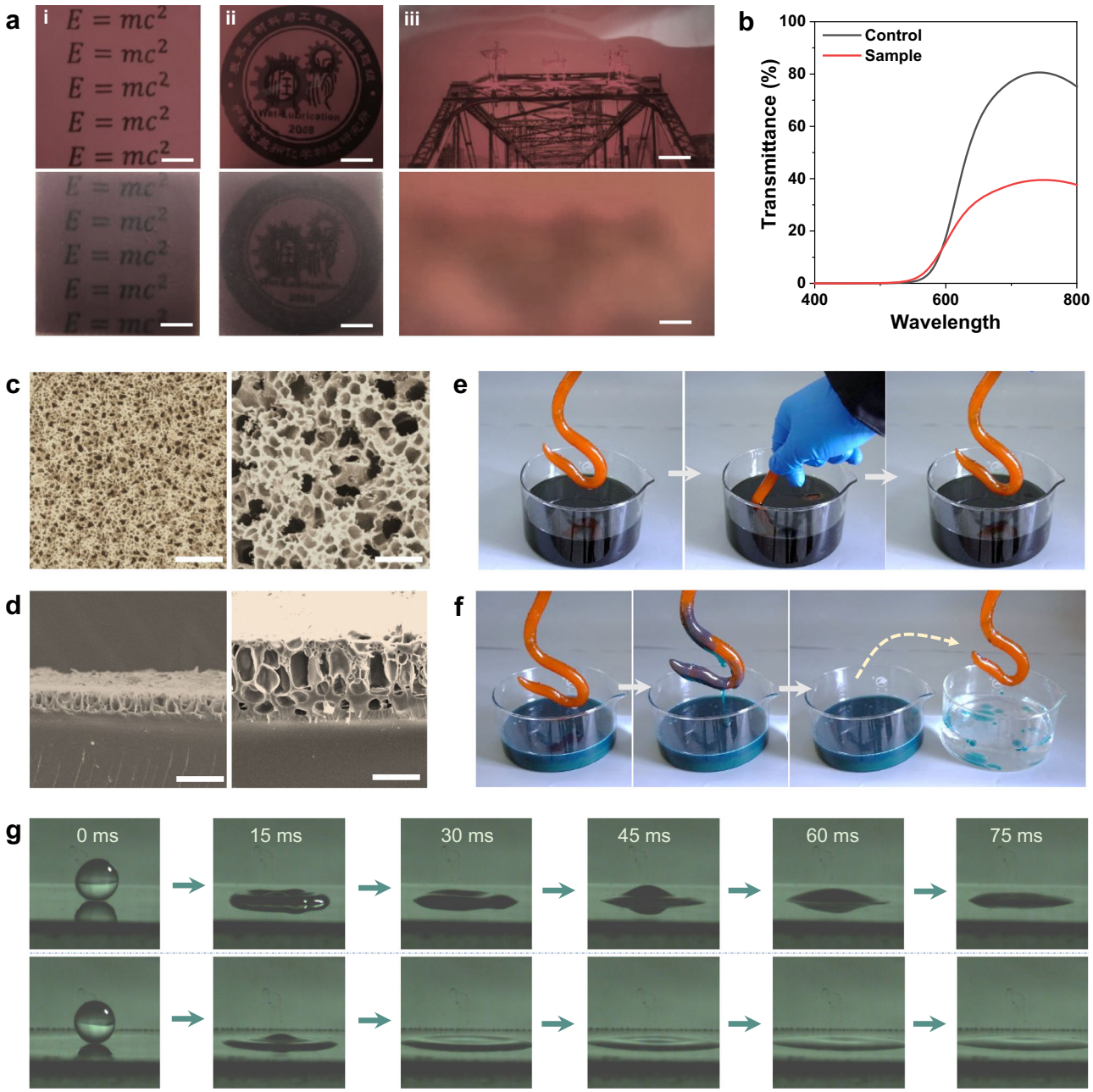

Fig. 2 | Characterizations of SLH. a Photographs of mechanically robust DN-hydrogel (top) and SLH (bottom) samples covered with different labels (i-formula, ii-logo, iii-Lanzhou Zhongshan Bridge; scale bars: 4.0 mm, 4.0 mm, and 4.0 mm). **b**Transmittance curves of control (mechanically robust DN-hydrogel) and SLH samples. **c** Local (left, scale: 100 μm) and enlarged (right, scale: 50 μm) surface SEM images of MS-SLH. **d** Local (left, scale: 100 μm) and enlarged (right, scale: 50 μm) cross-sectional SEM images of SLH. **e** Demonstration showing the anti-fouling performance of artificial SLH earthworms upon immersion in a dyed vegetable oil bath. **f** Demonstration showing the anti-fouling performance of artificial SLH earthworms upon immersion in a dyed heavy oil bath and rinsing with water. **g** Dynamic wetting process of a water droplet (10 μL) on the surface of a mechanically robust DN-hydrogel (top) and an SLH sample (bottom) recorded by a high-speed camera.

dissociation layer and its load-bearing capacity, the optimal conditions for manufacturing layered super-lubrication hydrogel (SLH) are determined (dissociation concentration: 10%, dissociation time: 2 h).

Next, the lubrication feature, load-bearing capacity, and lifespan of the SLH are systematically evaluated by employing a typical face-to-face contact mode under with a reciprocating sliding style (Experimental methods: 3.7). The test results show that the friction coefficients of the SLH samples are both less than 0.01 (super-lubrication: SL) for dissociation concentrations of 10% and 20% (Fig. 3e), whereas the similar SL behavior is observed when the dissociation time is less than 8 h (Fig. 3f). The lowest friction coefficient is attained as low as ~0.003 for the SLH sample under optimal conditions (dissociation concentration: 10%, dissociation time: 2 h) and reaches as low as ~0.003. Subsequently, the load-bearing capacity of SLH is systematically investigated (Fig. 3g). The average friction coefficient of optimal SLH sample is always below 0.004 when the normal load does not exceed 60 N (contact pressure: 8.48 MPa). When the normal load increases to 70 N (contact pressure: 9.90 MPa), the friction coefficient slightly increases to 0.006. However, the SL behavior of SLH sample can still be observed at high normal load conditions (80 N, contact pressure: 11.32 MPa). To the best of our knowledge, the SLH system has the highest load-bearing capacity and lifespan among all of the

https://doi.org/10.1038/s41467-024-55715-8

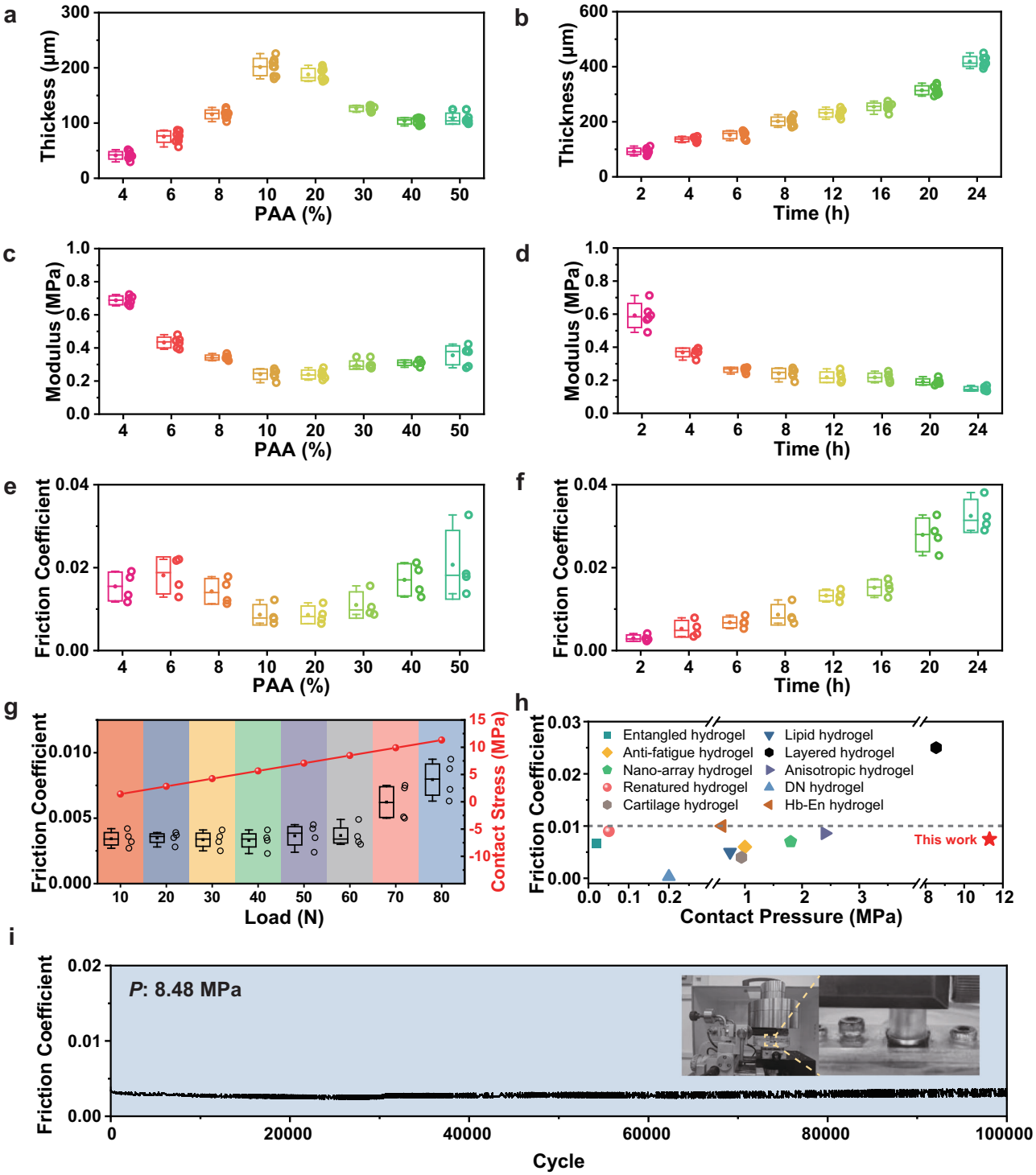

Fig. 3 | Control of the dissociation-layer thickness, mechanical strength and lubrication performance of SLH. a Evolution of the dissociation layer thickness with the PAA concentration at a certain treatment time of 8 h. **b** Evolution of the dissociation layer thickness with the PAA treatment time at a certain concentration of 10%. **c** Evolution of the dissociation-lubrication layer modulus with the PAA concentration at a certain treatment time of 8 h. **d** Evolution of the dissociation-layer modulus with the PAA treatment time at a certain concentration of 10%. **e** Evolution of the surface friction coefficient for the dissociation layer with the PAA concentration at a certain treatment time of 8 h. **f** Evolution of the friction coefficient for the dissociation layer with the PAA treatment time at a certain concentration of 10%. **g** Changes in the surface friction coefficients and contact stresses for the dissociation layer under different normal loads. **h** Comparisons of the friction coefficient and contact pressure between the reported lubricous hydrogels and those used in this work. **i** Real-time and long-period (100,000 cycles) friction coefficient curve for the SLH sample under a high contact pressure of 8.48 MPa (treatment time: 2 h, PAA concentration: 10%). Note: for all box plots, the horizontal line within box represents the data value located in the middle sequence number, the upward bar represents the maximum data value and the downward bar represents the minimum data value, solid dot within box represents the average value.

reported SL hydrogel material systems (Fig. 3h), including entangled hydrogel,[30] lipid hydrogel,[31] anti-fatigue hydrogel,[48] layered hydrogel,[16] nano-array hydrogel,[32] anisotropic hydrogel,[33] renatured hydrogel,[49] DN hydrogel,[28,29] cartilage hydrogel,[40] Hb-En hydrogel.[47] Correspondingly, the lubrication lifespan of the SLH sample is evaluated. Within 100,000 testing cycles, the friction coefficient is always maintained at 0.003 under a high contact pressure of 8.48 MPa (Fig. 3i), and only slight surface wear is observed in the testing area (Supplementary Fig. 25), indicating the very strong SL robustness of our SLH system.

The mechanisms responsible for robust SL behavior can be analyzed as follows. First, when two pieces of hydrogel samples slide against each other, the existing typical microstructures of periodic but non-regular wrinkles prevent the mechanical interlocking of two sliding surfaces in the shearing process, which may reduce the real contact areas to achieve a low friction force contribution. Second, the carboxyl groups (-COOH) on the surface of the SLH sample dissociate to produce a large number of carboxylate ions ($-COO^-$), endowing the two sliding substrates with strong negative charges (Supplementary Figs. 26-27). The strong electrostatic repulsion effect at the sliding interface is a prerequisite for achieving ultralow friction coefficient, which can be effectively explained by current models.[17,32,33] Third, the large thickness of the dissociation lubrication layer ensures a strong surface hydration degree,[21,26,27], and its excellent mechanical properties ensure good wear resistance. Fourth, the porous feature of the dissociated lubrication layer ensures the rapid formation of a continuous lubrication phase during dynamic shearing processes.[19,20,24] In addition, due to its typical soft–hard composite characteristics, the SLH sample shows the extraordinary mechanical load-bearing capacity from the cartilage-like stress buffering effect under high contact pressure conditions,[58] which is the key to achieving a long lifespan of SL behavior. However, due to the friction complexity of the soft elastomers,[18] the durable SL behavior of the current system may be attributed to a combination of interfacial interactions, hydration effects, contact mechanics, rheology, and soft matter tribology.[22,23]

Characterization and lubricity evaluation of MS-SLH

To imitate the sustained lubricity feature of earthworm skin in the quasi-wet state environment, cylindrical texture pores are manufactured on the surface of the SLH sample by laser etching to function as gland-like pockets for storing lubricants, and then a multilevel structural super-lubrication hydrogel (MS-SLH) sample is successfully prepared. As observed from the optical microscopy results, the sufficient swelling of the dissociated-lubrication layer of MS-SLH in water induces the evident shrinkage of the texture porthole, resulting in the formation of a biomimetic gland-like structure in earthworms (Fig. 4a-left). However, the size of the texture porthole increases obviously when the dissociated-lubrication layer is in a "dry" state (Fig. 4a-right), resulting from partial dehydration. Accompanied by the occurrence of dehydration process, the size (radius) of the texture porthole gradually increases and remains unchanged after 10 min later (Fig. 4b). The results from the surface white-light 3D imaging system further verify this dynamic process (Fig. 4c). Importantly, this swelling and dehydration-induced behavior between closed pores and open pores is completely reversible (Fig. 4d). The real-time cross-sectional morphology evolution of the cylindrical texture porthole for the MS-SLH sample during the dynamic dehydration process is successfully captured (Fig. 4e). In the complete hydration state, the dissociated-lubrication layer generates sufficient swelling to close the pores. With the ongoing of dehydration, the thickness and volume of the dissociated-lubrication layer both decrease, and the pores gradually open.

As deduced, due to the spatial confinement effect, these pores are able to effectively prevent water evaporation during the dynamic shear process, and thus a longer lubrication lifespan is attained. Correspondingly, MS-SLH samples with different surface texture pore ratios are manufactured, while the sustained lubricity lifespans of them are evaluated systematically under a limited lubricant (water, 5 μL) (Fig. 4f). Compared with the non-textured SLH sample (0% pore ratio), increasing the pore ratio of surface pores is highly beneficial for achieving a longer SL period (Fig. 4g). Typically, the average duration of super-lubrication of the SLH sample is only 980 s, whereas this duration is extended 2700 s for MS-SLH sample with a 20% pore ratio (Fig. 4h). Furthermore, 5 μL of three kinds of lubricants with different viscosities, including water, hyaluronic acid (HA) and sodium alginate (SAA) are used to explore the duration of the super-lubrication state for the MS-SLH samples with 20% pore ratio (Fig. 4i, j). Notably, when 5 μL of SAA is used as a lubricant, the duration of super-lubrication state can reach as long as 3900 s (Fig. 4k). These results indicate that the manufacture of lubricants with high pore ratios and the use of high-viscosity water-retaining lubricants are suitable to attain a longer super-lubrication lifespan in earthworm-like quasi-wet environments. This phenomenon is also closely related to the shear-thinning characteristics of the lubricants themselves during the friction process (Supplementary Fig. 28).

The existing surface wrinkle patterns and textured pores could effectively reduce the real contact area to achieve a low friction force. The pores themselves serve as gland-like pockets to create a strong confinement space to greatly reduce the volatilization rate of the lubricant, whereas the lubricant stored within the pores of the texture pores can quickly migrate to form a hydration film at the friction interface during the dynamic shearing process. Correspondingly, the state evolution of the contacted interface under different normal loads could be simulated and observed by employing a self-built equipment (Supplementary Figs. 29, 30), in which the real contact area and calibrated contact pressures could be obtained (Supplementary Fig. 31). Compared with the apparent contact pressures, the calibrated contact pressures based on the reduced contact area (Sc) at different normal loads slightly increase. This concept ~~vividly~~ simulates the continuous lubricant migration behavior of epidermis skins in a non-pressurized state,[50–52] as well as "tribological rehydration" effect of natural cartilage layer for achieving dynamic lubricant supply implemented through mechanical loading and shearing.[59] This mechanism can be defined as "lubricant self-pumping". Therefore, the mechanism responsible for the extraordinary SL behavior if the MS-SLH sample can be further analyzed. Under low contact pressure conditions, the SL behavior is dominated mainly by the hydration lubrication mechanism. In contrast, at high contact pressures, the synergistic effects of the hydration lubrication mechanism and shear-induced self-pumping effect support the robust SL behavior (Supplementary Fig. 32). Different from traditional hard lubricant-composite surfaces and nonpermeable elastomer systems, an in-depth understanding of the interface lubrication mechanism of the MS-SLH system may rely on new theoretical models that combine surface chemistry, multiscale contact mechanics and hydrodynamics.

Demonstrations of mechanically robust lubricity for MS-SLH

As expected, due to its SL characteristic, MS-SLH has low friction–motion resistance against other contacted surfaces. An intuitive demonstration is performed by employing a weight (200 g) to slide against the surface of tilted glass sheets equipped with a MS-SLH sample, and the textured DN hydrogel without a dissociated-lubrication layer is used as a control (Supplementary Movie 1 and Movie 2). The weight has difficulty sliding off the surface of the control sample, even when the inclination angle of 14° (Fig. 5a). However, the weight can easily slide off the surface of the MS-SLH sample at a very low inclination angle of 3° (Fig. 5b). To visually demonstrate the mechanically robust SL characteristics of the MS-SLH sample, a home-made mechanical loading-monitoring system is manufactured (Fig. 5c–i). Specifically, 6 MS-SLH cylindrical sheets (Φ3 mm) are placed on the bottom of a movable loading system with a cargo-loading pool, and then slide against a MS-SLH track (35 mm × 200 mm) lubricated by water (Fig. 5c-ii). With the directional movement of the

https://doi.org/10.1038/s41467-024-55715-8

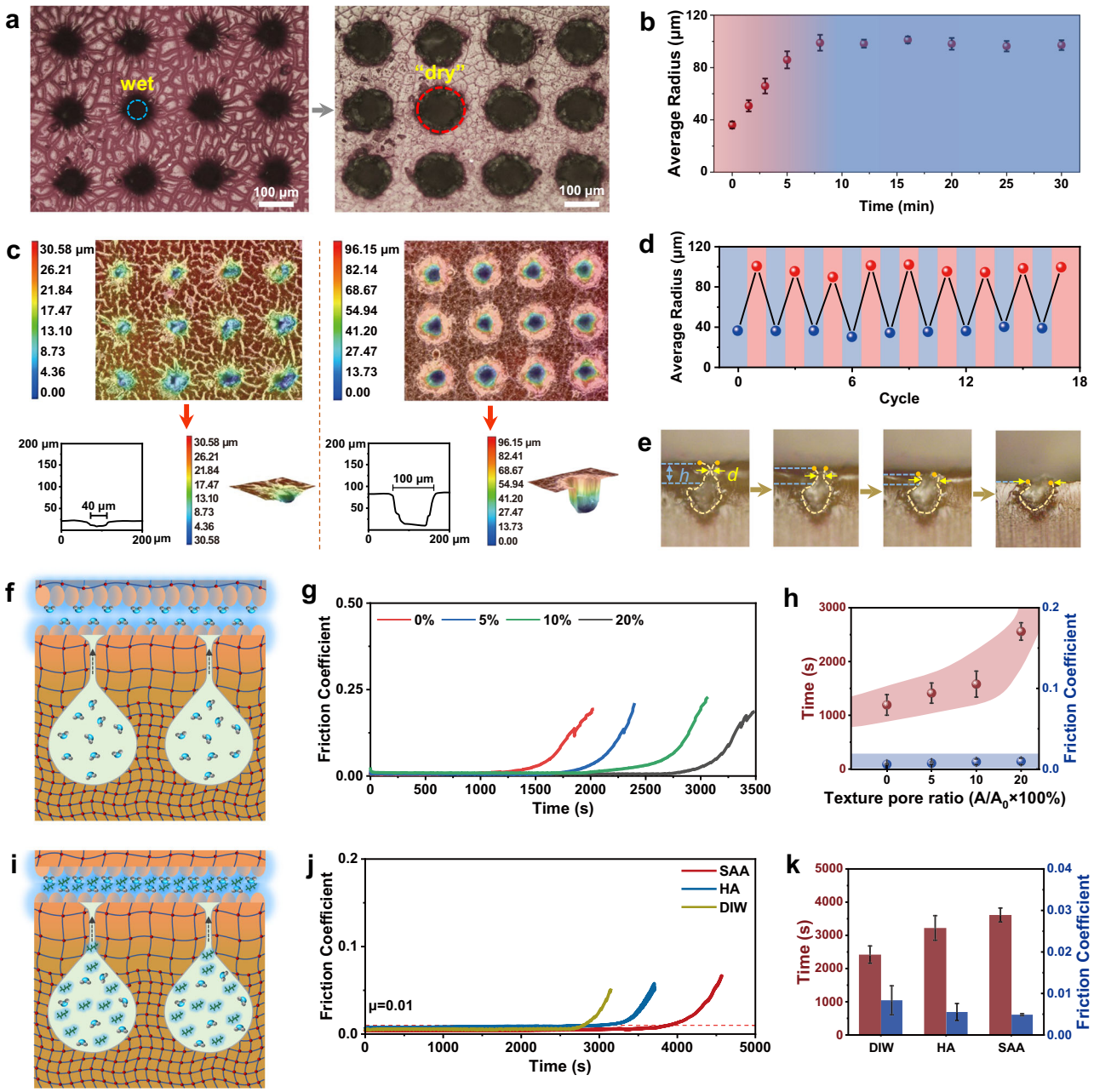

Fig. 4 | Characterization and lubricity evaluation of MS-SLH. a Evolution of the surface optical morphology from the wet state to the "dry" state for MS-SLH (scale: 100 μm). **b** Evolution of the surface texture pore size with dehydration time for MS-SLH ($n = 3$, mean ± SD). **c** Surface and cross-sectional 3D morphologies in the wet state and "dry" state for MS-SLH. **d** Reversible evolution of the surface texture pore size between at wet state and "dry" state for MS-SLH. **e** Snapshots recording the cross-sectional morphology evolution of a texture pore for MS-SLH during the dynamic dehydration process; here, *h* represents the swelling thickness of the dissociation–lubrication layer, *d* represents the size of the texture pore neck. **f** Schematic diagram showing the interface contact situation for the MS-SLH and MS-SLH regimes with deionized water (DIW) as the swelling medium. **g** Evolution of the surface friction coefficients with sliding test time for the MS-SLH samples with different texture: pore ratios (0, 5, 10, 20%) (lubricant: DIW-5.0 μL, load: 40 N). **h** Effective retention time of the super-lubrication state along with the corresponding friction coefficients for the MS-SLH samples with different texture:pore ratios (0, 5, 10, 20%) (lubricant: DIW-5 μL) ($n = 3$, mean ± SD). **i** Schematic diagram showing the interface contact situation for MS-SLH and the MS-SLH regimes with DIW, HA and SAA as the swelling media. **j** Evolution of surface friction coefficients with sliding test time for the MS-SLH samples with a 20% texture:pore ratio (lubricant: DIW, HA and SAA-5.0 μL; load: 40 N). **k** Effective retention time of the superlubrication state along with corresponding friction coefficients for the MS-SLH samples with a 20% texture-to-pore ratio (lubricant: DIW, HA and SAA, 5 μL) ($n = 3$, mean ± SD).

loading system, sand is poured into the loading pool to achieve a simultaneous increase in the normal load. Correspondingly, the real-time signals of the friction force and normal load are recorded by the sensor, and the friction coefficient is obtained by dividing the friction force by the normal load (Supplementary Movie 3). As the normal load dynamically increases, the sliding interface can always maintain an SL state (Fig. 5d). Amazed, the maximum bearing load of the MS-SLH track could reach 498 N, with a local high contact pressure of 11.74 MPa along with low friction coefficient of 0.0074 (Fig. 5c-iii).

Furthermore, in order to demonstrate the long-lasting lubrication feature of MS-SLH, another home-made mechanical monitoring system is manufactured (Fig. 5e, Supplementary Movie 4). Specifically, a

https://doi.org/10.1038/s41467-024-55715-8

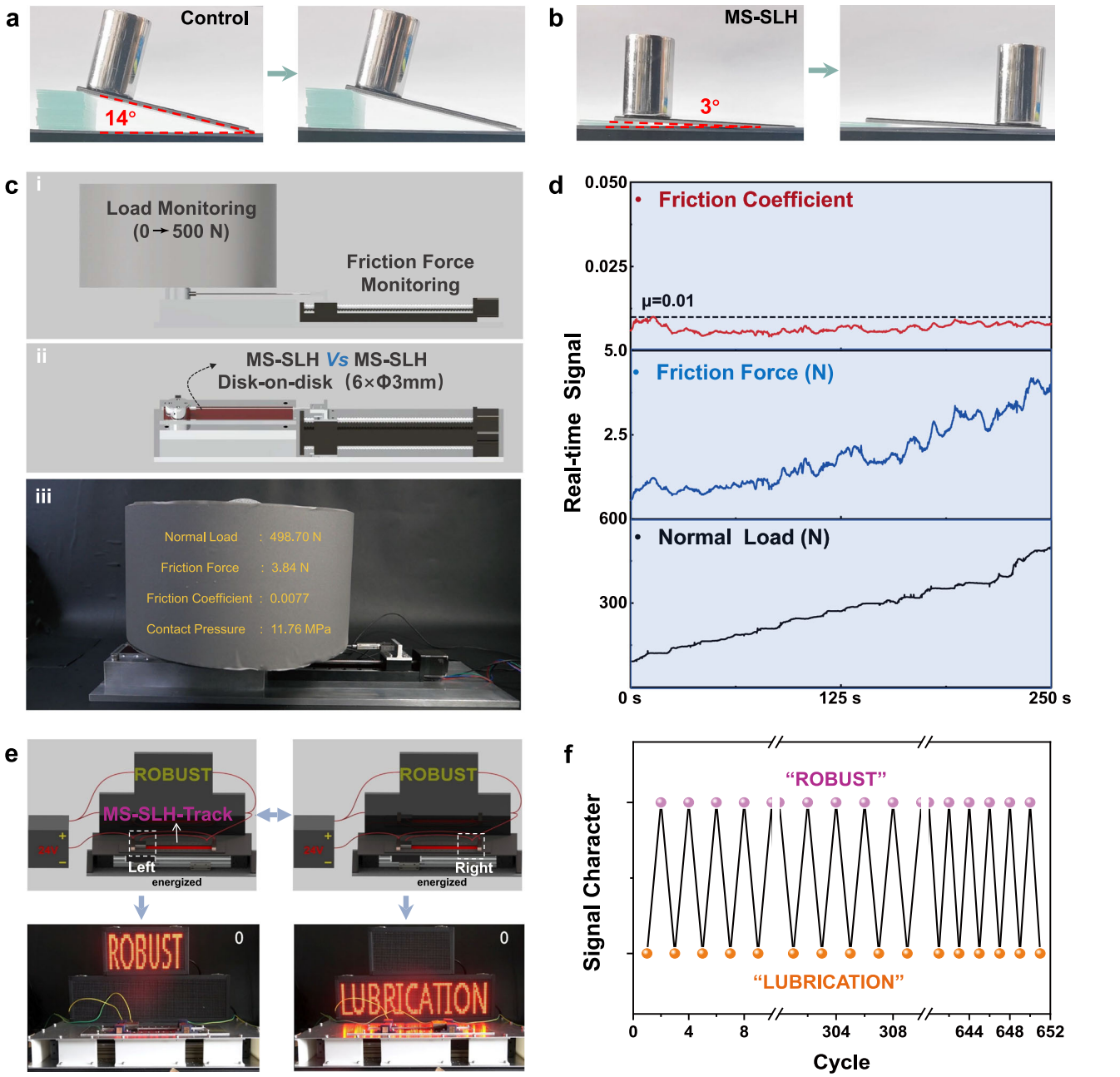

Fig. 5 | Intuitive demonstration of super-low friction, high load-bearing and long-lasting lubrication assisted with limited lubricant for MS-SLH. Weight sliding experiment on surface of tilted glass sheets equipped with (**a**) control sample (textured DN hydrogel) and (**b**) MS-SLH sample. **c** Directional movement of movable loading system (6×Φ3 mm, MS-SLH cylindrical sheet) on a MS-SLH track (35 mm × 200 mm) in response to increased normal loads from 0 to 500 N using a home-made mechanical monitoring system, and (**d**) data collection of real-time signals of friction efficiency, friction force and normal loads are recording. **e** Reciprocating motion of a conductive steel slider equipped with a square MS-SLH sheet (35 mm×35 mm) in air on an MS-SLH track (35 mm×180 mm) after swelling equilibrium in water without applying any extra lubricant, and (**f**) reversible signal display of the character between "ROBUST"-left and "LUBRICATION"-right using a home-made mechanical monitoring system.

conductive aluminum slider equipped with a square MS-SLH sheet (35 mm×35 mm) performs reciprocating motion in air on an MS-SLH track (35 mm × 180 mm). The MS-SLH track is directly used for testing after swelling equilibrium in water is reached, and the surface free water film is removed without any extra lubricant. A magnetic motion-control system is used to maintain a constant normal load. When the slider moves to the left sensor, the circuit is connected and the LED board displays a "Robust" character signal. When the slider moves to the right sensor, the circuit is connected and the LED board displays a "Lubrication" character signal. Surprisingly, the slider could run smoothly on the MS-SLH track for 651 cycles (Fig. 5f), due to the super-low friction feature and strong lubricant retention capacity of the texture pores.

Discussion

In this work, inspired by the lubricity durability of earthworms, we developed a multilevel structural super-lubrication hydrogel (MS-SLH) system (a self-pumping hydrogel) by chemically dissociating a double network hydrogel to generate a robust and wrinkled lubrication layer, and then followed by laser etching to construct cylindrical texture pores as gland-like pockets for storing lubricants. By precisely adjusting the concentration and dissociation time of the PAA etchant,

the microstructure, hydration degree, mechanical modulus, and thickness of the lubrication layer could be finely tuned, thereby obtaining the optimal parameters (concentration: 10%, time: 2 h) for achieving SL behavior. The dissociation lubrication layer of SLH exhibited fast but reversible hydration/dehydration process. The SLH shows a very low friction coefficient (~0.008) under high contact pressure conditions (*P:* 11.32 MPa) and durable SL lifespans as long as 100 k cycles. In particular, a high number of texture pores (pore ratio: 20%) creates a strong confinement space to store the lubricant, and ensures the durable migration of the lubricant to the moveable interface under the dynamic shearing process. As a result, the MS-SLH system demonstrates a sustained lubricity period (3700 cycles) by using a limited lubricant volume (5 μL) in air. This feature simulates the continuous lubricant migration behavior of epidermis skins and the cartilage layer to achieve dynamic lubricity maintenance. The synergistic effects of the hydration lubrication mechanism and shear-induced self-pumping effect support the robust SL behavior. Finally, the demonstration experiments based on self-built equipment intuitively exhibit robust and durable SL behavior of the MS-SLH system. This work provides an easy strategy for large-scale manufacturing of super-lubrication hydrogels, and can potentially be used to advance the engineering applications of high-performance water-lubrication coatings suitable for high-end medical devices.

Methods

Materials

Acrylic acid (AA, >99%, TCI), acrylamide (AAm, J&K Chemical Ltd.), α-ketoglutaric acid (>99.0%, Sigma-Aldrich). N,N′-methylenebisacrylamide (MBA, 99%) and ferric chloride hexahydrate ($FeCl_3{\cdot}6H_2O$) were purchased from Sinopharm, China. Hyaluronic acid (HA, 97%, 40–100 kDa, 3000-5000 mPa·s) and sodium alginate (SAA, viscosity: 1000–1200 mPa·s) were both purchased from Macklin Biochemical Technology Co. Ltd.

Samples preparation

Preparation of double-crosslinked hydrogel as mechanically robust matrix. Firstly, 4.2 g of acrylamide (AAm), 1.44 g of acrylic acid (AA), 11.7 mg of α- ketoglutaric acid and 18.4 mg of N,N′- methylene bisacrylamide (MBA) were dissolved into 20 mL of deionized water and stirred at room temperature for 5 min to form a uniform aqueous solution. Subsequently, nitrogen gas was injected into the aqueous solution to remove dissolved air and avoid the inhibitory effect of oxygen during the polymerization process. Next, the degassed aqueous solution was injected into two glass plate-constructed molds with a spacing of 1 mm, and then followed by UV irradiation (λ = 365 nm) for 45 min to obtain a chemically crosslinked hydrogel of P(AAm-AA). Afterwards, the prepared P(AAm-AA) hydrogel was immersed into a $FeCl_3{\cdot}6H_2O$ (0.25 mol/L) solution for 24 h to form a PAA/Fe^{3+} physical network. The residual components and uncoordinated Fe^{3+} were subsequently removed by soaking the sample into deionized water for 24 h to obtain a double crosslinked hydrogel of P(AAm-AA)/Fe.

Preparation of layered super-lubrication hydrogel (SLH). First, the P(AAm-AA)/Fe hydrogel was cut into a specific size (15 mm × 15 mm), then one side of it was adhered with 3 M tape and fixed with the acrylic plate, while the exposed side was used to construct the lubrication layer. Specifically, the exposed side of P(AAm-AA)/Fe hydrogel sheet was immersed into polyacrylic acid (PAA) solutions with different mass concentrations (49–50%) for specific durations (2–24 h), and then removed and immersed in deionized water for 24 h to remove residual polyacrylic acid macromolecules and dissociated Fe^{3+}. Correspondingly, a layered super-lubrication hydrogel (SLH) was obtained.

Preparation of earthworm-inspired multilevel structural super-lubrication hydrogel (MS-SLH). The super-lubrication hydrogel (SLH) sheet was bonded onto the stainless steel substrate with Loctite 496, and the surface dissociation layer was exposed to air for partial dehydration (note: the presence of a water film can weaken the laser). A picosecond laser microfabrication system (power: 18%, Suzhou Delong Laser Co., Ltd) was used to generate cylindrical texture pores (diameter: 100 μm) through the subsurface of super-lubrication hydrogel (SLH) sheet (the density of pores is defined as texture pore ratios of 0, 5, 10 and 20%, and was equal to $A/A_0 \times 100\%$, where A is the effective pore area and A_0 is the apparent area). Subsequently, the textured super-lubrication hydrogel (SLH) sheet was immersed into deionized water or lubricants bath for sufficient swelling, and then a multi-level structural super-lubrication hydrogel (MS-SLH) was successfully prepared.

Characterizations

Morphologies. The surface and cross-sectional morphologies of the SLH and MS-SLH samples in the completely swollen state were observed via an Olympus optical microscope (BX51). After in situ freeze-drying for 48 h (−80 °C, 1 Pa), the dry morphology of the samples was observed via field emission-scanning electron microscopy (FE-SEM, JSM-6701F, Japan). The surface and cross-sectional morphologies of the P(AAm-AA)/Fe sample were characterized using SEM (JSM5600LV, JEOL, Japan) at 20 kV. The quasi-wet state morphology of the P(AAm-AA)/Fe sample after swelling equilibrium was observed using atomic force microscopy (Bio-AFM, JPK Nanowizard4XP, Bruker, German) in quantitative imaging (QI) mode with an SNL-10 tip ($k = 0.108$ N m^{-1}).

Thickness and roughness of the lubrication layer. The thicknesses of the lubrication layer in the hydrated and dehydrated states of the samples were measured from the cross-sectional morphology using a standard ruler from the software of an Olympus Optical Microscope (BX51).

An optical imaging technique with a 3D VHX-6000 (Keinz Corporation, Japan) digital microscope was used to measure the surface roughness of the samples in the swollen state ($n = 8$, measurements were taken from distinct samples), along with the depth and surface 3D morphology of the samples in the hydrated and dehydrated states.

Wettability. The dynamic fast wetting process of a water droplet (10.0 μL) on the surface of a sample (bottom) was recorded by a high-speed camera (UP-Lambda, Rtec Instruments). The contact angle (CA) of a water droplet (5.0 μL) on the surface of a sample was obtained with a DSA100 instrument (Germany, KRUSS) ($n = 7$, measurements were taken from distinct samples).

The water content of the lubrication layer was measured via the following method. The mass (m_1) of the control sample without the lubrication layer and the mass of the SLH sample (m_2) of the same size (15 mm × 15 mm) were measured in the equilibrium swelling state, and the water content of the lubrication layer was defined as $(m_2\text{-}m_1)/m_2 \times 100\%$ ($n = 3$, measurements were taken from distinct samples).

Zeta potential. The surface potential difference of the sample was measured via a solid surface zeta potential analyzer (SurPASS-3, Anton Paar). The sample size was 20 mm×10 mm, and a KCl electrolyte solution (1.0 mmol/L) was used as the test liquid (pH = 7.0) ($n = 5$, measurements were taken from distinct samples).

Mechanical properties. The surface mechanical modulus of the SLH samples was measured with a bioindenter (UNHT^3 Bio, Anton Paar) ($n = 6$, measurements were taken from distinct samples). The radius of the indenter (ruby ball) was 0.5 mm, and the applied load was 500 μN. For the P(AAm-AA)/Fe sample, the applied load increased to 1000 μN ($n = 5$, measurements were taken from distinct samples). The samples were fixed on a flat glass slide by Loctite 496 in all tests. All samples

were soaked into water for different durations to allow sufficient swelling before testing.

The rheological measurement of lubricants. The shear-thinning characteristics of HA and SA were investigated via rheological measurements (RS6000. HAAKE, Germany). All experiments were performed using a cone plate with a diameter of 35 mm at 25 °C. The viscosity–shear rate curves were recorded in the range of 0.05 to 5000 s^{-1}.

Friction performance. The friction performance was evaluated on a pin-on-disk tribometer (TRB, CSM, Anton Paar, Switzerland) by employing a typical face-to-face contact mode with reciprocating sliding style (distance: 10 mm, frequency: 1 Hz, load: 10, 20, 30, 40, 50, 60, 70, 80 N). A cylindrical hydrogel sheet (diameter: 3 mm, thickness: 1 mm) was used as a pin, whereas the square hydrogel sheet (length: 20 mm, width: 20 mm, thickness: 1 mm) was used as a disk. The lubricants used were water and the macromolecules (1% hyaluronic acid-HA and 1% sodium alginate-SAA). The friction coefficient is obtained by dividing the frictional force by the normal load.

Except for the lifespan evaluation and duration test, the number of friction test cycles for common experiments was 900 ($n = 3$, measurements were taken from distinct samples), whereas the number of friction test cycles for various loads was 600 ($n = 3$). The test temperature ranged from 25-28 °C, and the relative humidity (RH) was 20%. The wear morphology on the surface of the sample after 100,000 sliding cycles was observed via optical microscopy.

Investigation of the interface contact states under different normal loads. Dynamic observation equipment was built to indirectly obtain the real contact areas of the compressed friction contact interface of the MS-SLH sample under different normal loads (10 N, 20 N, 30 N, 40 N, and 45 N; the maximum load capacity of the sensor was 45 N), with consideration of the two key contributions from the wrinkle patterns and textured pores. To simulate the friction process more accurately, a transparent glass cylinder ($d = 3$ mm) was used as an indenter to interact with the MS-SLH sample. Considering the resolution problem of the optical images in the contacted area, we used reflection mode to obtain the contact area of MS-SLH. The contact area was calculated via pixel analysis of the optical photographs using ImageJ software. The pixel ratio for the contact area is defined as Ac (0 ~ 1), whereas the pixel ratio for the noncontact area is defined as 1-Ac. To obtain statistical error, each optical photograph was divided into four quadrants for analysis ($n = 4$, measurements were taken from distinct positions). The apparent contact areas of the MS-SLH samples at different normal loads were similar and defined as S_0 (7.065 mm^2), where Ac was 1. The measured contact area was defined as Sc, and the calibrated contact pressure was obtained. Due to the opacity of the MS-SLH sample, our custom-built equipment was only a simulation platform, and the attainment of accurate contact area data of the friction contact interface involving two sliding MS-SLH sheets was difficult.

Demonstrations

Weight sliding experiment (Movies 1 and 2). The MS-SLH sample and control hydrogel sample (textured DN hydrogel without a dissociated-lubrication layer) were fixed onto the titled glass substrate. The inclination angle of control hydrogel sample-fixed glass substrate was 14°, whereas it decreased to 3° for the MS-SLH-fixed glass substrate. An intuitive demonstration was performed by employing a weight (200 g) to slide against on the surface of the tilted glass sheets equipped with different samples.

Directional movement of the movable loading system at the super-lubrication interface (Movie 3). To visually demonstrate the mechanically robust super-lubrication characteristics of MS-SLH, a custom-made system including a mechanical loading part (A) and a monitoring sensor part (B) was manufactured. Six MS-SLH cylindrical sheets (Φ3 mm) were placed on the bottom platform of the movable loading part with a cargo loading tank and then slid against an MS-SLH track (35 mm×200 mm). The lubricant was water. With the directional movement of the loading system, sand was continuously poured into the loading pool to achieve a synchronous increase in the normal load from 0 N to 498.70 N (11.76 MPa). Correspondingly, the real-time signals of the friction force and normal load were recorded by the monitoring sensor. The displacement moving part was driven by a screw slide using a motor, with a speed of 0.5 mm/s. The interface friction coefficient was obtained by dividing the friction force by the normal load.

Long-lasting lubrication feature of MS-SLH (Movie 4). To more intuitively demonstrate the long-lasting lubrication feature of MS-SLH, another home-made mechanical monitoring system was developed and was driven mainly by the bottom slide track (35 mm×180 mm). A strong magnetic magnet above the slide rail was applied, while the MS-SLH sheet (35 mm×35 mm) was fixed below the iron block. The strong magnetic attraction force drove the iron block to move and caused the MS-SLH-fixed iron block to rub back and forth. Copper blocks were set at the left and right ends as conductive sensors, which triggered the fast display of characters ("Robust" and "lubrication") on the LED board.

Reporting summary

Further information on research design is available in the Nature Portfolio Reporting Summary linked to this article.

Data availability

The data supporting the findings of this study are available within the paper, Supplementary Information, and Supplementary Movies. The data generated in this study have been deposited in the Figshare repository (https://doi.org/10.6084/m9.figshare.27304683). The raw data underlying the figures are available in the file Source Data. Source data are provided with this paper.

References

1. Klein, J. Repair or replacement-a joint perspective. *Science* **323**, 47–48 (2009).
2. Lee, S. & Spencer, N. D. Sweet, hairy, soft, and slippery. *Science* **319**, 575–576 (2008).
3. Neu, C. P., Komvopoulos, K. & Reddi, A. H. The interface of functional biotribology and regenerative medicine in synovial joints. *Tissue Eng. B-Rev.* **14**, 235–247 (2008).
4. Jahn, S. & Klein, J. Lubrication of articular cartilage. *Phys. Today* **71**, 48–54 (2018).
5. Jahn, S., Seror, J. & Klein, J. Lubrication of articular cartilage. *Annu. Rev. Biomed. Eng.* **18**, 235–258 (2016).
6. Fan, H. L. & Gong, J. P. Fabrication of bioinspired hydrogels: challenges and opportunities. *Macromolecules* **53**, 2769–2782 (2020).
7. Adibnia, V. et al. Bioinspired polymers for lubrication and wear resistance. *Prog. Polym. Sci.* **110**, 101298 (2020).
8. Lin, W. F. & Klein, J. Hydration lubrication in biomedical applications: from cartilage to hydrogels. *Acc. Mater. Res.* **3**, 213–223 (2022).
9. Li, W. Z., Lai, J. Y., Zu, Y. & Lai, P. X. Cartilage-inspired hydrogel lubrication strategy. *Innovation* **3**, 100275 (2022).
10. Lin, W. F. & Klein, J. Recent progress in cartilage lubrication. *Adv. Mater.* **33**, 2005513 (2021).
11. Liu, L. et al. Meniscus-inspired self-lubricating and friction-responsive hydrogels for protecting articular cartilage and improving exercise. *ACS Nano* **17**, 24308–24319 (2023).
12. Chen, Q. et al. Bilayer hydrogels with low friction and high load-bearing capacity by mimicking the oriented hierarchical structure of cartilage. *ACS Appl. Mater. Interfaces* **14**, 52347–52358 (2022).

13. Liao, I.-C., Moutos, F. T., Estes, B. T., Zhao, X. H. & Guilak, F. Tissue engineering: composite three-dimensional woven scaffolds with interpenetrating network hydrogels to create functional synthetic articular cartilage. *Adv. Funct. Mater.* **23**, 5825 (2013).
14. Kamata, H., Akagi, Y., Kayasuga-Kariya, Y., Chung, U. I. & Sakai, T. Nonswellable" hydrogel without mechanical hysteresis. *Science* **343**, 873–875 (2014).
15. Zhao, Z. G., Fang, R. C., Rong, Q. F. & Liu, M. J. Bioinspired nanocomposite hydrogels with highly ordered structures. *Adv. Mater.* **29**, 1703045 (2017).
16. Rong, M. M. et al. High lubricity meets load capacity: cartilage mimicking bilayer structure by brushing up stiff hydrogels from subsurface. *Adv. Funct. Mater.* **30**, 2004062 (2020).
17. Gong, J. P. & Osada, Y. Gel friction: A model based on surface repulsion and adsorption. *J. Chem. Phys.* **109**, 8062–8068 (1998).
18. Gong, J. P. Friction and lubrication of hydrogels—its richness and complexity. *Soft Matter* **2**, 544–552 (2006).
19. Pitenis, A. A. et al. Polymer fluctuation lubrication in hydrogel gemini interfaces. *Soft Matter* **10**, 8955–8962 (2014).
20. Cuccia, N. L., Pothineni, S., Wu, B., Harper, J. M. & Burton, J. C. Pore-size dependence and slow relaxation of hydrogel friction on smooth surfaces. *Proc. Natl Acad. Sci. USA.* **117**, 11247–11256 (2020).
21. Ma, L. R., Gaisinskaya-Kipnis, A., Kampf, N. & Klein, J. Origins of hydration lubrication. *Nat. Commun.* **6**, 6060 (2015).
22. Kim, J. & Dunn, A. C. Generalized rate-and-state model linking rheology and soft matter tribology. *Extrem. Mech. Lett.* **41**, 101013 (2020).
23. Oogaki, S. et al. Friction between like-charged hydrogels—combined mechanisms of boundary, hydrated and elastohydrodynamic lubrication. *Soft Matter* **5**, 1879–1887 (2009).
24. Porte, E., Cann, P. & Masen, M. A lubrication replenishment theory for hydrogels. *Soft Matter* **16**, 10290–10300 (2020).
25. Shoaib, T. & Espinosa-Marzal, R. M. Advances in Understanding hydrogel lubrication. *Colloid Interfac.* **4**, 54 (2020).
26. Gaisinskaya, A. et al. Hydration lubrication: exploring a new paradigm. *Faraday Discuss.* **156**, 217–233 (2012).
27. Jahn, S. & Klein, J. Hydration Lubrication: The macromolecular domain. *Macromolecules* **48**, 5059–5075 (2015).
28. Gong, J. P. et al. Synthesis of hydrogels with extremely low surface friction. *J. Am. Ceram. Soc.* **123**, 5582–5583. (2001).
29. Kaneko, D., Tada, T., Kurokawa, T., Gong, J. P. & Osada, Y. Mechanically Strong Hydrogels with ultra-low frictional coefficients. *Adv. Mater.* **17**, 535–538 (2005).
30. Kim, J., Zhang, G. G., Shi, M. X. Z. & Suo, Z. G. Fracture, fatigue, and friction of polymers in which entanglements greatly outnumber cross-links. *Science* **374**, 212–216 (2021).
31. Lin, W. et al. Cartilage-inspired, lipid-based boundary-lubricated hydrogels. *Science* **370**, 335–338 (2020).
32. Ma, S. H. et al. Nanoporous Substrate-Infiltrated Hydrogels: a bioinspired regenerable surface for high load bearing and tunable friction. *Adv. Funct. Mater.* **25**, 7366–7374 (2015).
33. Liu, H. et al. Robust super-lubricity for novel cartilage prototype inspired by scallion leaf architecture, *Adv. Funct. Mater.* **34**, 2310271 (2024).
34. Ren, H. Y., Guo, A. D. & Luo, C. H. Sandwich hydrogel to realize cartilage-mimetic structures and performances from polyvinyl alcohol, chitosan and sodium hyaluronate. *Carbohyd. Polym.* **328**, 121738 (2023). Article.
35. Schmidt, T. A. Lubricating lipids in hydrogels. *Science* **370**, 288–289 (2020).
36. Tong, Z. M. et al. Hagfish-inspired smart SLIPS marine antifouling coating based on supramolecular: lubrication modes responsively switching and self-healing properties. *Adv. Funct. Mater.* **32**, 2201290 (2022).
37. Kang, J. Y. et al. Mucosa-inspired electro-responsive lubricating supramolecular-covalent hydrogel. *Adv. Mater.* **35**, 2307705 (2023).
38. Zhang, Y. L. et al. Modulus adaptive lubricating prototype inspired by instant muscle hardening mechanism of catfish skin. *Nat. Commun.* **13**, 377 (2022).
39. Wang, J. et al. Semi-convertible hydrogel enabled photoresponsive lubrication. *Matter* **4**, 675–687 (2021).
40. Huang, J. J. et al. One-pot construction of articular cartilage-like hydrogel coating for durable aqueous lubrication, *Adv. Mater.* **36**, 2309141 (2024).
41. Yu, Y. et al. Multifunctional "Hydrogel Skins" on diverse polymers with arbitrary shapes. *Adv. Mater.* **31**, 1807101 (2019).
42. Kim, Y., Parada, G. A., Liu, S. D. & Zhao, X. H. Ferromagnetic soft continuum robots. *Sci. Robot.* **4**, eaax7329 (2019).
43. Bai, M. H. et al. Mucosa-like conformal hydrogel coating for aqueous lubrication. *Adv. Mater.* **34**, 2108848 (2022).
44. Takahashi, R. et al. Tough particle-based double network hydrogels for functional solid surface coatings. *Adv. Mater. Interfaces* **5**, 1801018 (2018).
45. Xu, R. N. et al. A universal strategy for growing a tenacious hydrogel coating from a sticky initiation layer. *Adv. Mater.* **34**, 2108889 (2022).
46. Zhang, Y. L. et al. Successive Redox-reaction-triggered interface radical polymerization for growing hydrogel coatings on diverse substrates. *Angew. Chem. Int. Ed.* **61**, e202209741 (2022).
47. Wang, Z. B. et al. Hydrogen bonds-pinned entanglement blunting the interfacial crack of hydrogel–elastomer hybrids, *Adv. Mater.*, 2313177. (2024)
48. Liu, J. et al. Fatigue-resistant adhesion of hydrogels. *Nat. Commun.* **11**, 1071 (2020).
49. Yang, Z. X. et al. Renatured hydrogel painting. *Sci. Adv.* **7**, eabf9117 (2021).
50. Laird, J. M., Kroger, M. & Heddleson, M. R. Earthworms. *Crit. Rev. Environ. Sci. Tech.* **11**, 189–218 (1981).
51. Ren, L. Q., Tong, J., Li, J. Q. & Chen, B. C. Soil adhesion and biomimetics of soil-engaging components: a Review. *J. Agric. Eng. Res.* **79**, 239–263 (2001).
52. Zhang, D. G. et al. Earthworm epidermal mucus: Rheological behavior reveals drag-reducing characteristics in soil. *Soil Tillage Res.* **158**, 57–66 (2016).
53. Gao, F. G., Kamali, E. B., Shirtcliffe, N. & Nield, C. T. A Preliminary study of the surface properties of earthworms and their relations to non-stain behaviour. *J. Bionic. Eng.* **7**, 13–18 (2010).
54. Zhao, H. X., Sun, Q. Q., Deng, X. & Cui, J. X. Earthworm-inspired rough polymer coatings with self-replenishing lubrication for adaptive friction-reduction and antifouling surfaces. *Adv. Mater.* **30**, 1802141 (2018).
55. Yang, S., Khare, K. & Lin, P. C. Harnessing surface wrinkle patterns in soft matter. *Adv. Func. Mater.* **20**, 2550–2564 (2010).
56. Breid, D. & Crosby, A. J. Effect of stress state on wrinkle morphology. *Soft Matter* **7**, 4490–4496 (2011).
57. Liu, N. et al. Wrinkled interfaces: taking advantage of anisotropic wrinkling to periodically pattern polymer surfaces. *Adv. Sci.* **10**, 2207210 (2023).
58. Greene, G. W. et al. Adaptive mechanically controlled lubrication mechanism found in articular joints. *Proc. Natl Acad. Sci. USA.* **108**, 5255–5259 (2011).
59. Moore, A. C. & Burris, D. L. Tribological rehydration of cartilage and its potential role in preserving joint health. *Osteoarthr. Cartil.* **25**, 99–107 (2017).

Acknowledgements

S. M. acknowledges financial support from Strategic Priority Research Program of the Chinese Academy of Sciences (No. XDB 0470201), the National Natural Science Foundation of China (NSFC; No. 52075522 and 52322506), the Major Science and Technology Project of Gansu

Province (No. 23ZDGA011), and the West Light Foundation of The Chinese Academy of Sciences (No. xbzg-zdsys–202211). F. Z. was funded by NSFC (No. 22032006) and the Key Research Project of Shandong Provincial Natural Science Foundation (No. ZR2021ZD27), B. Y. was funded by the Gansu Province Basic Research Innovation Group Project (No. 22JR5RA093). Jacob Klein (Weizmann Institute of Science) assisted with the discussions for the experimental results and gave technical guidance.

Author contributions

S. M. and F. Z. conceived the idea and designed the experimental protocol. L. L. and S. M. performed and completed the entire experimental studies. W. Z., R. L., X. Z., and Y. Z. provided necessary experimental help. S. M. organized the Figures and wrote the draft. B. Y. and Y. L. gave technical suggestions. S. M. and F. Z. revised and finalized the manuscript. S. M. and L. L. contributed equally to this work.

Competing interests

The authors declare no competing interests.

Additional information

Supplementary information The online version contains supplementary material available at https://doi.org/10.1038/s41467-024-55715-8.

Correspondence and requests for materials should be addressed to Ying Liu or Feng Zhou.

Peer review information *Nature Communications* thanks Alison Dunn and the other, anonymous, reviewers for their contribution to the peer review of this work. A peer review file is available.